Rapid Rise of Sea Level 19,000 Years Ago and Its Global Implications

Peter U. Clark,[1*] A. Marshall McCabe,[3] Alan C. Mix,[2] Andrew J. Weaver[4]

Evidence from the Irish Sea basin supports the existence of an abrupt rise in sea level (meltwater pulse) at 19,000 years before the present (B.P.). Climate records indicate a large reduction in the strength of North Atlantic Deep Water formation and attendant cooling of the North Atlantic at this time, indicating a source of the meltwater pulse from one or more Northern Hemisphere ice sheets. Warming of the tropical Atlantic and Pacific oceans and the Southern Hemisphere also began at 19,000 years B.P. These responses identify mechanisms responsible for the propagation of deglacial climate signals to the Southern Hemisphere and tropics while maintaining a cold climate in the Northern Hemisphere.

Records of sea level change derived from sediment cores from the Bonaparte Gulf, Australia, indicate that the Last Glacial Maximum (LGM) lowstand was abruptly terminated by a rapid sea level rise of 10 to 15 m at 19,000 years B.P. (1) (Fig. 1). (Unless otherwise indicated, all ages are reported in calendar years.) This 19,000-year meltwater pulse (19-ky MWP) indicates partial collapse of one or more ice sheets, with an attendant large and rapid flux of fresh water to the ocean that, depending on its duration, would have ranged from 0.25 to 2 Sv (1 Sv = 10^6 m³ s⁻¹) over 100 to 500 years. Dynamical ocean models demonstrate that the thermohaline circulation (THC) is sensitive to freshwater perturbations on the order of 0.1 Sv (2, 3), indicating that the 19-ky MWP, if released in areas of deep water formation, would have perturbed the THC. However, the source of the 19-ky MWP and its potential effect on climate remain unknown. Moreover, the very existence of the 19-ky MWP has been questioned because no dated samples from a lone Bonaparte Gulf core confirm the proposed rapid rise of sea level (4).
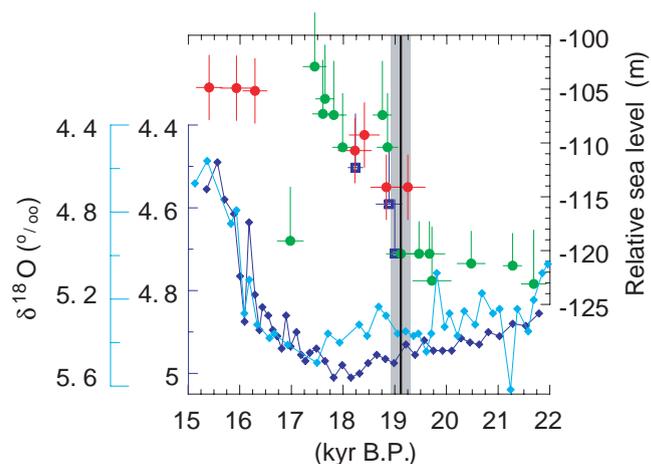
We first document evidence in support of the 19-ky MWP from a site along the Irish Sea coast. In particular, the combination of early local deglaciation, a relatively low marine limit, and isostatic emergence of the Irish Sea coast established conditions favorable for preserving evidence of a subsequent rapid rise of sea level at 19,000 years B.P., if such an event occurred.

Radiocarbon dates on raised marine sediments and cosmogenic dates on boulders from glacial moraines indicate that initial deglaciation of the British-Irish Ice Sheet (BIIS) in Ireland began ≥20,000 years B.P. (5). Because the BIIS is located in a region that is particularly sensitive to changes in North Atlantic climate, we infer that this early deglaciation occurred in response to an increase in the Atlantic meridional overturning (AMO) and the associated warming of the North Atlantic region that began 21,000 to 22,000 years B.P. (6, 7). Alternatively, because warming the atmosphere in a glacial climate could have enhanced precipitation sufficiently to lead to a more positive mass balance and thus growth of the ice sheets (8), initial deglaciation of the BIIS may instead have been triggered by relative sea level rise associated with isostatic subsidence. In any event, the maximum BIIS stored <2 m of sea level equivalent, so that any corresponding changes in its size related to initial deglaciation ≥20,000 years B.P. are too small to be discernible in current records of global sea level change (Fig. 1).

Early deglaciation of coastal regions was accompanied by a high relative sea level due to isostatic depression by the BIIS (9). The marine limit on the western margin of the Irish Sea Basin near Kilkeel, Northern Ireland (Fig. 2) is 30 m above sea level (asl) and formed between ~21,000 and 19,000 years B.P. Global sea level was 130 to 140 m lower than at present during this time (1), indicating that the marine limit at Kilkeel records a net isostatic uplift of 160 to 170 m.

After the deglaciation of the Irish Sea coast at Kilkeel, eastward-flowing rivers draining the Mourne Mountains eroded several broad (~200 m wide) and deep (~10 m) channels into existing stratified glaciomarine sediments (Fig. 2) (10). These channels were graded to a relative sea level equivalent to or lower than present (Fig. 2), indicating that the coast had isostatically emerged at least 30 m (the marine limit) by the time they had formed.

Evidence that sea level subsequently rose is suggested by thick fossiliferous marine muds that now fill the erosional channels to a level ~10 m asl (Fig. 2). We used accelerator mass spectrometry (AMS) ¹⁴C to date five samples of the foraminifera *Elphidium clavatum* that were collected at four levels from near the base to the top of the muds that fill one channel (Fig. 2 and Table 1) (11). The five ages indicate rapid sedimentation of the muds; radiocarbon ages at the base are statistically the same (at 1σ) as the radiocarbon age at the top of the sequence. We take the weighted mean of the calibrated radiocarbon ages (Table 1) to derive an age of 19,119 ± 180 years B.P. for this event (12).

Our new data from the Irish Sea coast thus confirm a rapid rise of sea level of at least 10 m at ~19,000 years B.P. that was previously inferred from Bonaparte Gulf (1) (Fig. 1). A clear signal of this event has not been described from benthic δ¹⁸O records (Fig. 1), but the expected change in seawater δ¹⁸O (reduction of ~0.1 per mil) may be partially masked by offsetting temperature effects (cooling of ~0.5°C) associated with reduced deep water formation during the earliest phase of deglaciation.

[1]Department of Geosciences, [2]College of Oceanic and Atmospheric Sciences, Oregon State University, Corvallis, OR 97331, USA. [3]School of Environmental Studies, University of Ulster, Coleraine, Northern Ireland BT52 1SA, UK. [4]School of Earth and Ocean Sciences, University of Victoria, P.O. Box 3055, Victoria, British Columbia V8W 3P6, Canada.
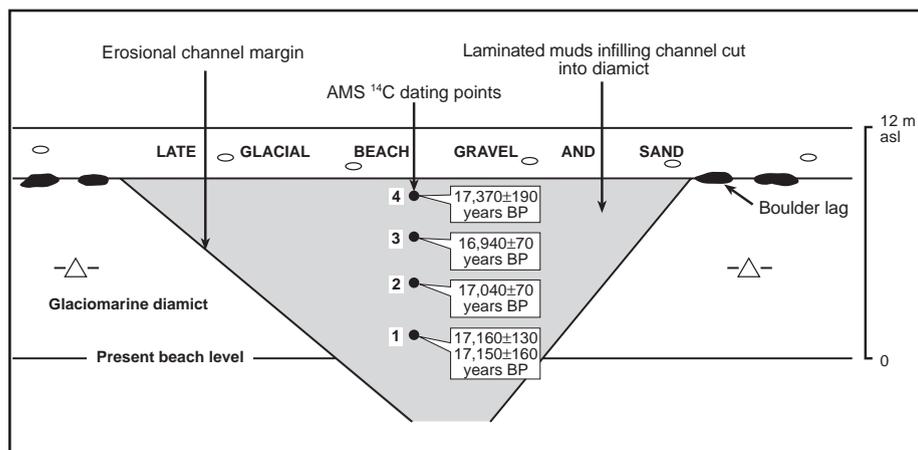
*To whom correspondence should be addressed. E-mail: clarkp@geo.oregonstate.edu

Fig. 1. Plot of far-field relative sea level indicators from Bonaparte Gulf (green circles) (1), Barbados (blue squares) (14), and Sunda Shelf (red circles) (33), indicating an abrupt 10- to 15-m rise in global sea level 19,000 years B.P. The vertical bar represents the weighted mean calibrated age (19,119 ± 180 years B.P.) of our radiocarbon ages constraining a rapid sea level rise on the Irish Sea coast (Fig. 2 and Table 1). Also shown are benthic oxygen isotope records from North Atlantic core NA 87-22 (light blue diamonds, far left axis, water depth 2161 m) (34) and Pacific core W8709A-13PC (dark blue diamonds, near left axis, water depth 2712 m) (35).

Fig. 2. Schematic diagram of the mud-filled channel at Kilkeel steps (54°03′N, 6°00′W) from which radiocarbon ages were obtained (Table 1). The channel was eroded by easterly flowing streams into glaciomarine diamicton, filled with fossiliferous marine sediments after sea level rise, and then truncated by a late-glacial shoreline on which was deposited beach sand and gravel.
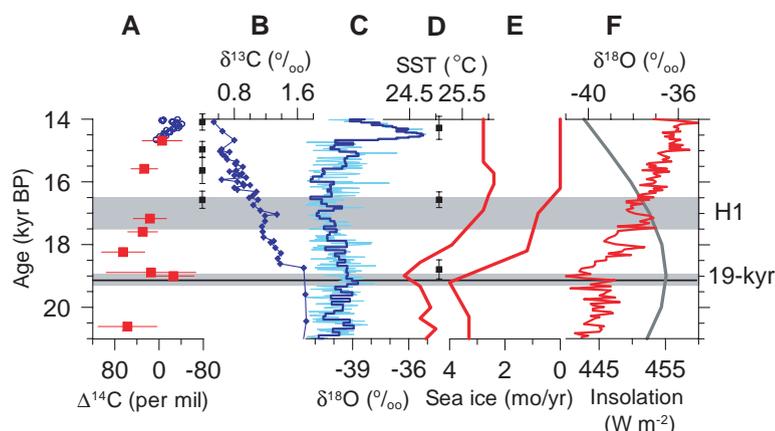
Fig. 3. Proxy records from the Atlantic basin and Antarctica showing initiation of a thermal seesaw (cooling in the north, warming in the south) at the time of the 19-ky MWP. (**A**) Linearly detrended record of atmospheric $\Delta^{14}C$ from corals (red squares) (14) and Cariaco basin (blue circles) (15). (**B**) Record of benthic $\delta^{13}C$ from North Atlantic core SO75-26KL (36). Positions of calibrated radiocarbon ages used to construct age model are shown by filled squares (1σ error). (**C**) Record of $\delta^{18}O$ from GISP2 ice core (6, 37). (**D**) Record of SSTs derived from alkenones from tropical Atlantic core M35003-4 (38). Positions of calibrated radiocarbon ages used to construct age model are shown by filled squares (1σ error). (**E**) Record of duration of sea ice (months per year) from South Atlantic core TN057-13-PC4 (39). (**F**) Record of $\delta^{18}O$ from the Byrd ice core (40, 41). Also shown as solid gray line is mid-month January insolation at 65°S (42), showing that high southern latitude insolation begins to decrease at a time when temperatures begin to increase. Horizontal gray bars represent timing of H1 and of the 19-ky MWP, as suggested by the Irish Sea data.

Table 1. AMS ^{14}C ages from Kilkeel, Northern Ireland. Sample elevations are measured from base of exposure. Radiocarbon ages are AMS ^{14}C ages from monospecific samples of *E. clavatum* in marine muds. Calibrated ages were calculated with Calib 4.4 (http://radiocarbon.pa.qub.ac.uk/calib) and a ΔR (the local reservoir age anomaly) of 600 ± 200 years (11).

Laboratory number	Sample elevation (m)	Radiocarbon age (years)	Calibrated age (years)
CAMS-89688	8.5	17,370 ± 190	19,409 ± 373
CAMS-89687	6.5	16,940 ± 70	18,915 ± 302
CAMS-89686	4	17,040 ± 70	19,030 ± 304
AA22352	1.3	17,150 ± 160	19,156 ± 349
AA22351	1.3	17,160 ± 130	19,168 ± 332

Although evidence exists for deglaciation earlier than 19,000 years B.P., including that from the BIIS (5), the 19-ky MWP is important in identifying the termination of the LGM associated with partial collapse of one or more ice sheets, as measured by the first rise of global sea level (1). Moreover, this event may have had a substantial impact on the strength of North Atlantic Deep Water (NADW) formation (and hence the strength of the AMO), depending on the source of the ice and its entry point into the ocean. It is unlikely to have had a substantial effect on Labrador Sea Water (LSW) formation, as the LSW/NADW stratification characteristic of the late Holocene Labrador Sea likely never developed during the glacial cycle (13).

With a duration of ≤500 years, a 10-m eustatic rise would correspond to a freshwater flux of ≥0.25 Sv. Our Irish Sea data indicate that the sea level rise may have been considerably shorter than 500 years. Given the demonstrated sensitivity of NADW formation to freshwater forcing, a freshwater flux of this magnitude would be associated with a reduction in the AMO. Lower resolution coral data (14) identify a rapid and large (~100 per mil) increase in atmospheric radiocarbon ($\Delta^{14}C_{atm}$) at 19,000 years B.P. (Fig. 3A), similar in magnitude to that associated with the start of the Younger Dryas cold interval (15) and consistent with temporary stratification of part of the upper ocean. Because changes in the strength of NADW (and its preformed properties) dominate variations in $\Delta^{14}C_{atm}$ associated with the global carbon cycle at these time scales, the large increase in $\Delta^{14}C_{atm}$ at 19,000 years B.P. would be consistent with a large decrease in the AMO, arising from a decrease in NADW (and not LSW) formation in response to the 19-ky MWP.

Additional evidence provides further support for a reduction in the AMO and attendant ocean heat transport associated with the 19-ky MWP. Geochemical data and climate models suggest that during the LGM, NADW shoaled to depths of less than 2000 m (16, 17). A benthic $\delta^{13}C$ record from 1100 m water depth off Portugal (18) documents enhanced ventilation of middepth levels during the LGM (Fig. 3B), consistent with these results. However, benthic $\delta^{13}C$ values decreased abruptly at 19,000 years B.P., indicating a rapid reduction in water mass ventilation. Records of North Atlantic climate (Fig. 3C) suggest the start of a prolonged cooling (the Oldest Dryas) in response to reduced AMO at this time. Finally, we note that a peak in ice-rafted debris (IRD) occurs throughout the North Atlantic and the Nordic Seas at 19,000 years B.P., with IRD petrology indicating possible sources for the event from the Greenland, Iceland, and Fennoscandian ice sheets (19, 20).

Observations and modeling suggest several mechanisms by which a reduced AMO may rapidly induce far-field effects. Because

the AMO causes northward heat transport in the Atlantic basin, a reduction in the AMO should induce a compensatory warming in the tropical Atlantic and Southern Ocean (the bipolar thermal seesaw) (21), rapidly within the Atlantic but perhaps with a lag of several hundred years in the Southern Ocean (22). The initiation of warming at ~19,000 years B.P. at Atlantic and Antarctic sites (Fig. 3, D to F) records this expected ocean response to the 19-ky MWP. In particular, we note that warming occurred at Antarctic sites before any substantial rise in atmospheric CO_2 (23) and despite a gradual decrease in austral summer insolation (Fig. 3F), suggesting a dominant influence by the thermal seesaw and related feedbacks on the climate of the high southern latitudes at this time. For example, increased Southern Ocean sea surface temperatures (SSTs) caused sea ice meltback (Fig. 3E), leading to additional warming through positive ice-albedo feedback and exposure of the atmosphere to the underlying ocean.

Coupled ocean-atmosphere models have demonstrated that a SST anomaly imposed in the South Pacific will subduct along isopycnal surfaces into the equatorial thermocline and then upwell in the equatorial Pacific on a time scale of tens of years (24–26). Equatorial upwelling of a thermal anomaly then initiates a positive feedback between the tropical ocean and the atmosphere through the effects of the winds, thus amplifying an initial perturbation. Equatorward transmission of South Pacific SSTs may account for at least half of the changes in the equatorial Pacific at the LGM (26) and throughout the last ~150,000 years (27). These results provide a mechanism to explain near-synchronous early deglacial warming of equatorial Pacific SSTs with Antarctic warming at 19,000 years B.P. (Fig. 4, A and B).

Oceanographic observations suggest that equatorward ventilation may also be an important mechanism through which geochemical anomalies from high southern latitudes are rapidly transmitted to the equatorial Pacific (28). Spero and Lea (29) invoked this mechanism to explain the synchronous onset of a decrease in the $\delta^{13}C$ of dissolved inorganic carbon from the eastern equatorial Pacific with Antarctic warming during the last deglaciation. Specifically, Southern Ocean warming and attendant sea ice meltback led to enhanced upwelling of nutrient-rich, isotopically light Southern Ocean deep water (30). Newly upwelled waters transmitted their light $\delta^{13}C$ signal to shallow intermediate waters, which subsequently reached the equatorial Pacific to produce the signal measured in planktonic foraminifera. We documented this effect in greater detail (Fig. 4C and Table 2) and found a shift to lower planktonic $\delta^{13}C$ coincident with warming of the western Pacific warm pool after ~19,000 years B.P.

Newly upwelled Southern Ocean water transmitted to the equator in the shallow subsurface would also have been supersaturated with respect to CO_2. The partial pressure of CO_2 (PCO_2) of equatorial Pacific surface waters should have thus risen in association with warming of these isotopically lighter, CO_2-enriched waters. Indeed, a recent record from the western equatorial Pacific identifies changes of PCO_2 of surface waters that are synchronous with changes of SSTs and $\delta^{13}C$ (Fig. 4D). Although Palmer and Pearson (31) attributed these changes to more frequent and/or intense La Niña conditions associated with high northern latitude interstadials, within the dating resolution of the records, PCO_2 of Pacific surface waters changes synchronously with Antarctic warming (Fig. 4, A and D), thus corresponding to northern latitude stadials (Fig. 3, C and F).

We conclude that the 19-ky MWP originating in the Northern Hemisphere contributed to early deglacial warming in the Southern Hemisphere and the tropics while maintaining a cold Northern Hemisphere through its effect on the AMO and ocean heat transport. In particular—insofar as Southern Ocean warming is understood as a seesaw response to a reduced AMO, amplified by sea ice meltback—we suggest that subsequent oceanic teleconnections involving rapid equatorward ventilation represent one important control on equatorial Pacific SST and PCO_2 changes. These responses to the 19-ky MWP would have been reinforced by the subsequent freshwater forcing associated with Heinrich event 1 (H1) at 17,500 years B.P. (Figs. 3 and 4). Tropical warming induced by these oceanic responses may then have represented an important feedback on subsequent high-latitude deglaciation.

The sequence of events during the last deglaciation depicts a tightly coupled oceanic system that is sensitive to large freshwater forcings originating at both the northern and southern high latitudes (32). A challenge remains to partition those climate effects of high-latitude processes that propagate between hemispheres and to the tropics from those equatorial effects (such as El Niño–Southern Oscillation) that may operate independently of ice sheets and propagate poleward.
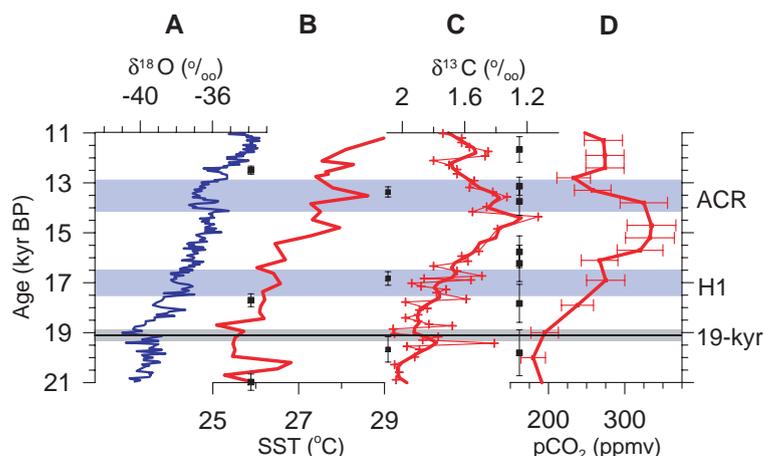
Fig. 4. Proxy records indicating near-synchronous transmission of thermal and geochemical anomalies from the Southern Ocean to the equatorial Pacific. (**A**) Record of $\delta^{18}O$ from the Byrd ice core (40, 41). (**B**) Record of SSTs derived from Mg/Ca from core MD9821-62 in the western equatorial Pacific (43). (**C**) Record of $\delta^{13}C$ from the planktonic foraminifera *Neogloboquadrina dutertrei* from marine core Y69-71P (0.083°N, 86.482°W, 2740 m depth). Positions of calibrated radiocarbon ages used to construct age model (Table 2) are shown by filled squares (1σ error). Thicker dark-red line represents data smoothed with a 1200-year Gaussian filter. (**D**) Record of PCO_2 (data points with error bars) from core ERDC-92 in the western equatorial Pacific (31). Positions of calibrated radiocarbon ages used to construct age model (44) are shown by filled squares (1σ error). Horizontal gray bars represent timing of the Antarctic Cold Reversal (ACR), H1, and the 19-ky MWP as suggested by the Irish Sea data.

Table 2. ^{14}C and calibrated ages from core Y69-71P, eastern equatorial Pacific Ocean. Calibrated ages were calculated with Calib 4.4 (http://radiocarbon.pa.qub.ac.uk/calib) and a ΔR of 167 ± 106 years.

Laboratory number	Sample type	Depth (cm)	Radiocarbon age (years)	Calibrated age (years)
OS 33894	*N. dutertrei*	50	9,760 ± 40	10,213 ± 153
(45)	Bulk CaCO₃	85	12,130 ± 180	13,363 ± 203
OS 33191	*N. dutertrei*	120	14,700 ± 65	16,827 ± 272
(45)	Bulk CaCO₃	165	17,170 ± 350	19,670 ± 509
OS 33895	*N. dutertrei*	180	19,150 ± 70	21,948 ± 365

References and Notes

1. Y. Yokoyama, K. Lambeck, P. De Deckker, P. Johnston, L. K. Fifield, *Nature* **406**, 713 (2000).
2. S. Manabe, R. J. Stouffer, *Paleoceanography* **12**, 321 (1997).
3. A. F. Fanning, A. J. Weaver, *Paleoceanography* **12**, 307 (1997).
4. I. Shennan, G. A. Milne, *Quat. Sci. Rev.* **22**, 1543 (2003).
5. D. Q. Bowen, F. M. Phillips, A. M. McCabe, P. C. Knutz, G. A. Sykes, *Quat. Sci. Rev.* **21**, 89 (2002).
6. P. M. Grootes, M. Stuiver, J. W. C. White, S. Johnsen, J. Jouzel, *Nature* **366**, 552 (1993).
7. E. Bard, F. Rostek, J.-L. Turon, S. Gendreau, *Science* **289**, 1321 (2000).
8. A. Schmittner, M. Yoshimori, A. J. Weaver, *Science* **295**, 1489 (2002).
9. A. M. McCabe, P. U. Clark, *Nature* **392**, 373 (1998).
10. The cut-and-fill nature of the channels suggests an erosional phase followed by a depositional phase, and the orientation of the channel axes suggests erosion by easterly flowing water draining the adjacent Mourne Mountains. We exclude a subglacial origin for the channels because they are eroded into glaciomarine sediments that were deposited subaqueously. The orientation of the channel axes perpendicular to the coast indicates that if the channels were eroded subaqueously during high relative sea level by a continuation of easterly flowing streams draining the adjacent Mourne Mountains, then there should be deltas deposited by these streams at the contemporaneous sea level. The absence of any such deltas, however, leads us to dismiss this possibility. We also exclude a subaqueous origin because there is no a priori reason why subaqueous processes would initially be erosional, followed by a switch to processes that result in nearly instantaneous infilling of the channels by sediments, particularly on low slopes and at shallow water depths (<30 m). We thus argue that a subaerial origin best explains the erosional phase, which we interpret as having occurred after initial deglaciation of the Kilkeel coast and subsequent isostatic emergence. Subsequent rapid deposition of marine sediments in the channels thus requires a rapid rise in eustatic sea level to flood the channels on what was otherwise still an isostatically emergent coast. The timing of local deglaciation (*5*) and the formation of the associated marine limit relative to the timing of channel filling (19,000 years B.P.) provides sufficient time for coastal emergence and subaerial channel erosion to occur.
11. The radiocarbon-dated fossil microfauna are dominated by the foraminifer *E. clavatum* (>90%) and the ostracod *Roundstonia globulifera* (5 to 10%). All foraminiferal tests are glassy and in pristine condition, including preservation of delicate ornamentation and of the last aperture. Valves of *R. globulifera* show intact instars, and valves of *Polycope* sp. are still attached.
12. Assuming a reservoir age correction of 400 years, our five radiocarbon ages have the same weighted mean ^{14}C age (16,640 ± 40 ^{14}C years B.P.) (at 2σ) as the weighted mean of three ^{14}C ages (16,360 ± 220 ^{14}C years B.P.) on a single sample of Barbados coral that has a corresponding weighted mean U/Th age of 19,000 ± 70 years B.P. (*14*). A larger reservoir age correction applied to our samples would improve this agreement. Independent calendar age constraints indicate that the reservoir age of North Atlantic surface waters increased substantially during cold periods of the last glaciation (*34*). On the basis of lower-end estimates of reservoir ages for the Younger Dryas (820 years) and H1 (1230 years) (*34*), we thus assume that a reservoir age of 1000 ± 200 years applies to the Oldest Dryas cold period initiated by the 19-ky MWP, and we calibrate our samples accordingly.
13. C. Hillaire-Marcel, A. de Vernal, G. Bilodeau, A. J. Weaver, *Nature* **410**, 1073 (2001).
14. E. Bard, M. Arnold, B. Hamelin, N. Tisnerat-Laborde, G. Cabioch, *Radiocarbon* **40**, 1085 (1998).
15. K. A. Hughen, J. R. Southon, S. J. Lehman, J. T. Overpeck, *Science* **290**, 1951 (2000).
16. J. C. Duplessy *et al.*, *Paleoceanography* **3**, 343 (1988).
17. A. J. Weaver, M. Eby, A. F. Fanning, E. C. Wiebe, *Nature* **394**, 847 (1998).
18. R. Zahn *et al.*, *Paleoceanography* **12**, 696 (1997).
19. G. Bond *et al.*, *Science* **278**, 1257 (1997).
20. M. Elliot, L. Labeyrie, T. Dokken, S. Manthe, *Earth Planet. Sci. Lett.* **194**, 151 (2001).
21. T. S. Stocker, D. G. Wright, W. S. Broecker, *Paleoceanography* **7**, 529 (1992).
22. A. Schmittner, O. Saenko, A. J. Weaver, *Quat. Sci. Rev.* **22**, 659 (2003).
23. E. Monnin *et al.*, *Science* **291**, 112 (2001).
24. D. F. Gu, S. G. H. Philander, *Science* **275**, 805 (1997).
25. A. J. Weaver, *Geophys. Res. Lett.* **26**, 743 (1999).
26. Z. Liu *et al.*, *Geophys. Res. Lett.* **29** (10), 10.1029/2001GL013938 (2002).
27. M. Feldberg, A. C. Mix, *Paleoceanography* **18** (1), 10.1029/2001PA000740 (2003).
28. J. R. Toggweiler, K. Dixon, W. S. Broecker, *J. Geophys. Res.* **96**, 20 (1991).
29. H. J. Spero, D. W. Lea, *Science* **296**, 522 (2002).
30. D. M. Sigman, E. A. Boyle, *Nature* **407**, 859 (2000).
31. M. R. Palmer, P. N. Pearson, *Science* **300**, 480 (2003).
32. A. J. Weaver, O. Saenko, P. U. Clark, J. X. Mitrovica, *Science* **299**, 1709 (2003).
33. T. Hanebuth, K. Stattegger, P. M. Grootes, *Science* **288**, 1033 (2000).
34. C. Waelbroeck *et al.*, *Nature* **412**, 724 (2001).
35. A. C. Mix *et al.*, in *Mechanisms of Global Climate Change at Millennial Time Scales*, P. U. Clark, R. S. Webb, L. D. Keigwin, Eds., vol. 112 of *Geophysical Monographs* (American Geophysical Union, Washington, DC, 1999), pp. 127–148.
36. R. Zahn *et al.*, *Paleoceanography* **12**, 696 (1997).
37. M. Stuiver, P. M. Grootes, *Quat. Res.* **53**, 277 (2000).
38. C. Ruhlemann, S. Mulitza, P. J. Muller, G. Wefer, R. Zahn, *Nature* **402**, 511 (1999).
39. A. Shemesh *et al.*, *Paleoceanography* **17** (4), 10.1029/2000PA000599 (2002).
40. S. J. Johnsen, W. Dansgaard, H. B. Clausen, C. C. Langway, *Nature* **235**, 429 (1972).
41. T. Blunier, E. J. Brook, *Science* **291**, 109 (2001).
42. A. Berger, M. F. Loutre, *Quat. Sci. Rev.* **10**, 297 (1991).
43. K. Visser, R. Thunell, L. Stott, *Nature* **421**, 152 (2003).
44. W. H. Berger, J. S. Killingley, *Mar. Geol.* **45**, 93 (1982).
45. M. G. Dinkleman, thesis, Oregon State University (1974).
46. We thank T. Guilderson and C. Bryant for providing AMS radiocarbon ages, and D. Bowen, S. Hostetler, and N. Pisias for helpful discussions. Supported by the University of Ulster (P.U.C. and A.M.M.), the NSF Earth System History program (P.U.C.) and Marine Geology and Geophysics program (A.C.M.), and the Canadian Natural Sciences and Engineering Research Council, the Killam Foundation, and the Canada Research Chair program (A.J.W.).

8 December 2003; accepted 16 April 2004

Wind as a Long-Distance Dispersal Vehicle in the Southern Hemisphere

Jesús Muñoz,[1]* Ángel M. Felicísimo,[2] Francisco Cabezas,[1] Ana R. Burgaz,[3] Isabel Martínez[4]

Anisotropic (direction-dependent) long-distance dispersal (LDD) by wind has been invoked to explain the strong floristic affinities shared among landmasses in the Southern Hemisphere. Its contribution has not yet been systematically tested because of the previous lack of global data on winds. We used global winds coverage from the National Aeronautics and Space Administration SeaWinds scatterometer to test whether floristic similarities of Southern Hemisphere moss, liverwort, lichen, and pteridophyte floras conform better with (i) the anisotropic LDD hypothesis, which predicts that connection by "wind highways" increases floristic similarities, or (ii) a direction-independent LDD hypothesis, which predicts that floristic similarities among sites increase with geographic proximity. We found a stronger correlation of floristic similarities with wind connectivity than with geographic proximities, which supports the idea that wind is a dispersal vehicle for many organisms in the Southern Hemisphere.

Dispersal mechanisms play a key role in determining plant and animal distributions. LDD, defined as passive transport by wind, storms, water flows, and other means (*1*), was proposed as early as 1845 (*2*) and is often invoked to explain biotic similarities between distant landmasses (*3–6*). However, some authors have questioned the likelihood of LDD by wind because it is so difficult to support the theory with experimental data (*7, 8*).

Here, we tested whether the shared floristic affinities among extratropical Southern Hemisphere landmasses can be explained by LDD of propagules by wind. We used data from the SeaWinds scatterometer (on board the QuikSCAT satellite) to model wind connectivity among landmasses and to test how well these wind highways explain the floristic similarities observed in four groups of cryptogams (mosses, liverworts, lichens, and pteridophytes). All four have both sexual and asexual propagules suitable for LDD, although the relative importance of each mode varies among the groups. The hypothesis that floristic similarities are due to wind dispersal

[1]Real Jardín Botánico, Plaza de Murillo 2, 28014 Madrid, Spain. [2]Escuela Politécnica, Universidad de Extremadura, 10071 Cáceres, Spain. [3]Departamento de Biología Vegetal I, Universidad Complutense, 28040 Madrid, Spain. [4]Ciencias Experimentales y Tecnología, Universidad Rey Juan Carlos, 28933 Móstoles, Spain.

*To whom correspondence should be addressed. E-mail: jmunoz@ma-rjb.csic.es